

Haptic Rendering and Psychophysical Evaluation of a Virtual Three-Dimensional Helical Spring

Vinithra Varadharajan*
The Robotics Institute

Roberta Klatzky†
Psychology Department

Bertram Unger‡
The Robotics Institute

Robert Swendsen§
Department of Physics

Ralph Hollis¶
The Robotics Institute
Carnegie Mellon University

ABSTRACT

This paper presents the development of a new deformable object for haptic interaction in the form of a 3D helical spring. This haptic and visual simulation is based on an analytical model of a quasistatic spring. The model provides a real-time computationally efficient method for rendering a deformable spring using a magnetic levitation haptic device. The solution includes equations for reaction forces and resisting moments experienced during compression, elongation, shear and tilting of the spring. The system is used to conduct psychophysical experiments that quantify human perception and discriminability of spring stiffness magnitude with and without vision and demonstrates the effectiveness of the device and the simulation for rendering springs. Experiment results show that spring magnitude perception follows a linear trend, and presence of vision enables better discrimination between different spring stiffnesses.

1 INTRODUCTION

There has been substantial interest in the virtual environment community in the haptic and visual modeling of deformable objects [5], [15]. One method of rendering elastic behavior in these models is by using a network of “Mass-Spring” elements [6]. Such models over-simplify the behavior of a deformable object. Another popular method is that of Finite Element Analysis (FEA) [2]. While FEA accurately captures continuous and nonlinear deformable behavior, it is also computationally intensive and unsuitable for real-time simulations. James and Pai have suggested pre-calculation methods [8], [9] to make FEA models computationally efficient. Such pre-calculated models have been used by Barbič and James [1] to identify the principal components of the deformation model and combine them appropriately to render a range of deformations and Mahvash and Hayward have used them in combination with interpolation techniques [13]. While these methods render real-time deformations, they compromise on accuracy and fidelity of the haptic interaction. In this paper, a method of rendering real-time, realistic and accurate haptic and visual 3D helical springs based on a quasistatic analytical model is presented. Equations that define the behavior of the spring during compression, elongation, shear and tilting, and that predict the buckling point are provided. Such a simulation is an initial step in the use of a magnetic levitation haptic device (MLHD) to render deformable objects. The simulation not only allows parameterization of the spring structure (e.g.,

length; coil diameter), material (e.g., Young’s modulus) and inherent qualities (e.g., compression rigidity constant), but also allows such parameterization in real time. Users can feel the results of parametric variations using free exploration and these variations are mapped into perceptible properties. Here we consider how users freely explore and perceive one fundamental property of a spring: its stiffness.

Interaction with a deformable object using a MLHD is equivalent to active exploration of a compliant object by contact with a rigid surface. Srinivasan and LaMotte [14] showed that humans can be quite effective at discriminating the compliance of objects and surfaces. Sensory information for this task comes from two sources: the skin (cutaneous) and the muscles, tendons and joints (kinesthesia). Srinivasan and LaMotte [14] also showed that kinesthesia is required for the discrimination among levels of compliance when springs are covered with a rigid surface. Furthermore, LaMotte [11] showed that people can discriminate stiffness even while wielding a tool when allowed active control. Vision also contributes to stiffness perception, as shown by Wu et al. [16], sometimes compensating for systematic bias in the haptic system. Indeed, Bingham et al. [4] showed that vision alone is sufficient for identifying spring motion, raising the issue of whether rendered forces will add to the realism of a stiffness model in which visual feedback of spring motion is present.

We used two classic psychophysical procedures to characterize perception of stiffness and to gauge the effectiveness of the spring simulation. One is magnitude estimation, which assesses how internal responses to the stiffness co-vary with rendered values. The other is the just noticeable difference procedure (JND), which assesses how perceptible small differences in stiffness are and how the perceptibility varies with the base stiffness value. One common finding in many perceptual domains is that the JND threshold is a constant proportion of the base value, following what is commonly called Weber’s law. Together, these measures describe stiffness perception over a broad range of supra-threshold values and at the limits of discrimination. Given the demands of fabricating real spring samples and the complexities of these procedures, it would not be possible to do such a study without the rendering capabilities of a MLHD, which makes it possible to generate high-resolution stiffness values over a broad range in the context of the ongoing experiment.

2 MAGNETIC LEVITATION HAPTIC DEVICE

A MLHD consists of a handle that is attached to a magnetically levitated flotor. Three photodiode sensors and LED beacons are used to monitor the position of the flotor. A MLHD provides maximum stiffness, k_{max} , of approximately 25 N/mm in translation and 50.0 Nm/rad in rotation. This stiffness refers to the performance limit in unilateral constraints while rendering rigid surfaces. The maximum force and the maximum moment generated ranges between 55 N to 140 N and between 6.3 Nm to 12.2 Nm respectively depending on the axis. These characteristics make a MLHD appropriate

*e-mail: vinithra.varadharajan@gmail.com

†e-mail: klatzky@cmu.edu

‡e-mail: bju@andrew.cmu.edu

§e-mail: swendsen@andrew.cmu.edu

¶e-mail: rhollis@cs.cmu.edu

for rendering springs since it is necessary in some cases to simulate high stiffnesses associated with “hard” springs and high moments experienced during buckling. Interaction with a 3D spring involves forces along the three axes of translation and moments about the three axes of rotation and thus requires a device with 6 degrees of freedom (DoFs). A MLHD satisfies this requirement since the 6-DoF motion of its handle has a range approximately that of comfortable fingertip motion with the wrist stationary (± 12 mm translation and $\pm 7^\circ$ rotation in all directions). In addition, a MLHD provides real-time position and orientation information with resolutions of 5-10 μm and high position bandwidth (≈ 125 Hz at ± 3 dB) [3].

3 RENDERING A 3D HELICAL SPRING

An analytical quasistatic model proposed by T.M. Lowery [12] was used to haptically and visually render the 3D helical spring. The model assumes a close-coiled helical compression spring with wire of circular cross section, and upper and lower end plates. Spring weight, seat friction, end-coil effects and the dynamics of a spring are not modeled by [12]. However, the inertia due to the 580 g mass of the flotor brings out dynamic characteristics of a spring such as oscillations with damping effect.

3.1 Haptic Rendering

The setup for the virtual simulation is that of a vertically positioned spring with its lower end plate fixed to the ground, as shown in Fig. 1. The user deforms the spring by applying forces and moments to the handle of a MLHD, which represents the upper end plate. The servo loop runs at a rate of 1000 Hz and the same rate is used to record the translation and rotation data of the handle. The coordinate system used in this paper refers to the Y axis as the vertical axis, while the X and Z axes define the horizontal plane. Subscripts refer to the respective translation axes.

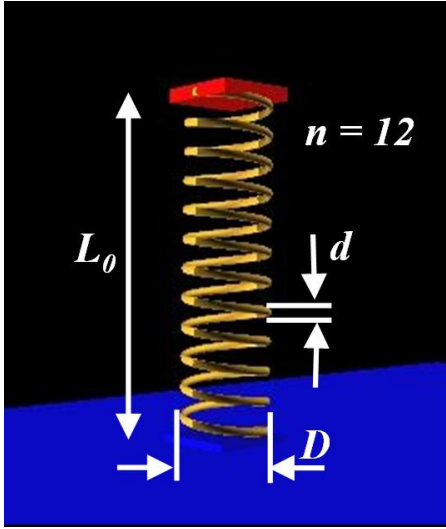


Figure 1: 3D view of undeformed spring.

The downward vertical motion range of the handle, V , is approximately 15mm in a MLHD. In the simulation, this depth corresponds to the free length of any spring, L_0 . Therefore, the vertical and horizontal translations obtained from the position sensors, $S_{X,Y,Z}$, are first transformed from real world coordinates to simulation coordinates, $T_{X,Y,Z}$, by

$$T_{X,Y,Z} = (S_{X,Y,Z}) \left(\frac{L_0}{V} \right). \quad (1)$$

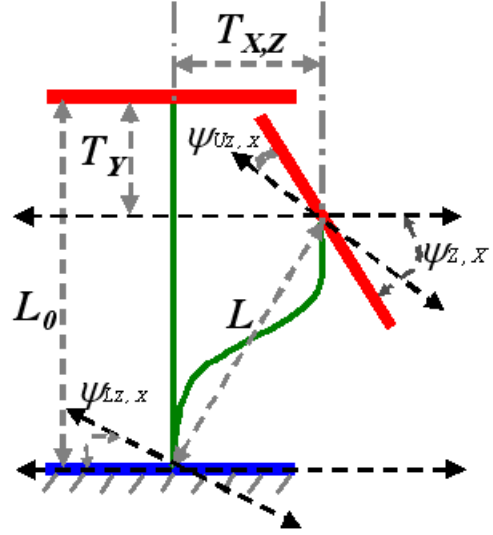


Figure 2: 2D view of spring angles and translations under deformation.

This enables the user to move the upper end plate through L_0 to reach the lower end plate in the simulation and at the same time reach the bottom of the motion range of the handle in the real world. T_Y is negative during compression and positive during elongation. The compressed length of the spring is calculated as the Euclidean distance between the upper end point of the spring centerline, $\{T_X, L_0 + T_Y, T_Z\}$, and the lower end point of the spring centerline, $\{0, 0, 0\}$,

$$L = \sqrt{T_X^2 + (L_0 + T_Y)^2 + T_Z^2}. \quad (2)$$

The pitch and roll angles of the flotor handle are computed from the sensor data. They are the angles of rotation of the upper end plate of the spring about the Z and X axes respectively (ψ_X, ψ_Z). The pitch and roll angles of the lower end plate are zero since it is held fixed. The angles of the spring centerline ends ($\psi_{U_x}, \psi_{L_x}, \psi_{U_z}$ and ψ_{L_z}) are the angles made by the normals to the end points of the spring centerline with the respective end plates. These angles are computed by

$$\psi_{L_z,x} = \tan^{-1} \left(\frac{T_{X,Z}}{T_Y} \right), \quad \text{and} \quad (3)$$

$$\psi_{U_z,x} = \psi_{L_z,x} - \psi_{Z,X}, \quad (4)$$

and are shown in Fig. 2.

The rigidity constants with respect to bending α , shear β , and compression γ , are given by

$$\alpha = \frac{L_0 d^4 E}{32 n D \left(1 + \frac{E}{2G} \right)}, \quad (5)$$

$$\beta = \frac{L_0 d^4 E}{8 n D^3}, \quad \text{and} \quad (6)$$

$$\gamma = \frac{L_0 d^4 G}{8 n D^3}, \quad \text{where} \quad (7)$$

α , β , and γ are the constants of proportionality relating applied moment and resulting curvature, applied shear force and resulting shear deformation, and applied vertical force and resulting compression, respectively [See Table I for symbol meanings]. The ver-

Table 1: Table of symbols

L_0	Free length of spring
L	Compressed length of spring
n	Number of active coils
d	Wire Diameter
D	Mean Coil Diameter
E	Young's Modulus
G	Shear Modulus
α	Rigidity constant with respect to bending
β	Rigidity constant with respect to shear
γ	Rigidity constant with respect to compression
k	Spring constant as defined by Hooke's law
P	Vertical reaction force
q	Buckling factor
$H_{X,Z}$	Horizontal reaction forces along X and Z axes respectively
$M_{U_{x,z}}$	Resisting moment at the upper end plate about X and Z axes respectively
$M_{L_{x,z}}$	Resisting moment at the lower end plate about X and Z axes respectively
$\psi_{X,Z}$	Pitch angle of upper end plate = Angle of rotation about X and Z axes respectively
$\psi_{U_{x,z}}$	Angles of the upper spring centerline end about the X and Z axis respectively
$\psi_{L_{x,z}}$	Angles of the lower spring centerline end about the X and Z axis respectively
V	Maximum vertical translation of MLHD
$T_{X,Y,Z}$	Translation along X, Y and Z axes respectively
$S_{X,Y,Z}$	Sensor data on translation along X, Y and Z axes respectively
$L_{buckling}$	Compressed length of the spring at which buckling occurs
$C_{X,Y,Z}$	3D coordinates of a point on the spring centerline

tical reaction force is given by

$$P = \gamma \frac{(L_0 - L)}{L_0}, \quad (8)$$

which is the familiar spring equation based on Hooke's law, where spring constant

$$k = \frac{\gamma}{L_0}. \quad (9)$$

A feedforward force with magnitude equal to the weight of the floor and in opposite direction to gravity was added to this vertical force. A spring buckles during compression when it deforms suddenly and nonlinearly along the vertical axis. The buckling factor is given by

$$q = \sqrt{\left| \frac{P}{\alpha} \left(1 + \frac{P}{\beta} \right) \right|}. \quad (10)$$

This factor predicts the buckling of parallel plates by

$$qL_0 = 2\pi. \quad (11)$$

At any point $\{C_X, C_Y, C_Z\}$, the vertical force, P , acts at a perpendicular distance of $C_{X,Z}$; the horizontal forces, $H_{X,Z}$, act at a perpendicular distance of $(L - C_Y)$; the moments, $M_{U_{z,x}}$, act at the upper end plate of the spring, as shown in Fig. 3. The moment, $M_{Z,X}$, acting at any point $\{C_X, C_Y, C_Z\}$ is given by

$$M_{Z,X} = C_{X,Z}P + H_{X,Z}(L - C_Y) + M_{U_{z,x}}. \quad (12)$$

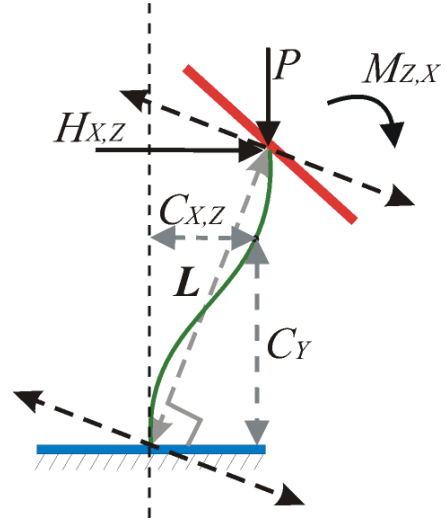


Figure 3: 2D view of forces and moments.

By relating the moments $M_{Z,X}$ as defined in eqn.(12) with the rigidity constant for bending (α), and by relating shear forces with the rigidity constant for shear (β), the expressions for the horizontal reaction forces and the resisting moments experienced at the end plates are derived. During compression, the horizontal reaction forces are

$$H_{X,Z} = \frac{P(\psi_{L_{z,x}} + \psi_{U_{z,x}})}{\frac{-LP}{q\alpha \tanh(\frac{qL}{2})} - 2}. \quad (13)$$

and the resisting moments experienced at the upper end plate are

$$M_{U_{z,x}} = \left[\left(\frac{H_{X,Z}}{P} + \psi_{U_{z,x}} \right) \alpha q - \frac{H_{X,Z}L}{\sin(qL)} \right] \cot\left(\frac{qL}{2}\right). \quad (14)$$

The development of a realistic deformable platform required definition of spring behavior during elongation as well. The equations defining elongation were derived as

$$H_{X,Z} = \frac{P(\psi_{U_{z,x}} + \psi_{L_{z,x}})}{\frac{-LP}{q\alpha \tanh(\frac{qL}{2})} - 2}, \text{ and} \quad (15)$$

$$M_{U_{z,x}} = \left[\left(\frac{H_{X,Z}}{P} + \psi_{U_{z,x}} \right) \alpha q + \frac{H_{X,Z}L}{\sinh(qL)} \right] \coth\left(\frac{qL}{2}\right). \quad (16)$$

In both compression and elongation, the resisting moments at the lower end plate are

$$M_{L_{z,x}} = M_{U_{z,x}} + H_{X,Z}L. \quad (17)$$

As $L \rightarrow L_0, P \rightarrow 0$ and $H_{X,Z} \rightarrow \infty$. The horizontal forces at this limit were derived as:

$$H_{X,Z} = \frac{-\beta(\psi_{U_{z,x}} + \psi_{L_{z,x}})}{2\left(1 + \frac{\beta L_0^2}{12\alpha}\right)}. \quad (18)$$

The resisting moment experienced upon rotation about the spring's vertical axis (yaw) is not defined by the analytical model in [12]. In this simulation it is modeled as a resisting torque proportional to the rotation. The difference between [12] and our simulation is that that the lower end plate in our simulation is not capable of rotation. This issue is addressed by making the computed forces in the simulation undergo a transformation of axes through ψ_{L_z} and

then through ψ_{Lx} . Commutativity of axes transformations is assumed since the angles are small. The moments experienced at the upper end plate as a result of these transformations are the sum of $M_{Uz,x}$ and $M_{Lz,x}$.

Using eqns. (8), (10) and (11), the compressed length at which buckling occurs can be expressed as

$$L_{buckling} = L_0 \left[1 - \frac{\beta}{2\gamma} \left(-1 + \sqrt{1 + \frac{16\pi^2\alpha}{\beta L_0^2}} \right) \right]. \quad (19)$$

A spring of lower stiffness has its buckling point higher than a very stiff spring, relative to the lower end plate. The behavior of the spring after buckling is not defined in [12]. A temporary solution was to set the horizontal forces and moments to zero and to scale down the vertical force. This renders an illusion of the spring bottoming out after buckling. Unseating of the spring, or slipping of the lower end plate, does not occur in this simulation because the lower end plate is held fixed.

A spherical boundary was implemented to keep the flotor within its sensor range. The boundary was modeled as a proportional-derivative controlled repulsive boundary. The derivative gain was set as a variable depending on the stiffness of the spring. The angle of rotation was limited to 2.86° . This limitation was necessary to keep the flotor within the sensor range in the cases where the resisting moments are very high.

3.2 Calibration along the Vertical Axis

Accurate and realistic haptic rendering of a deformable object required calibration of the MLHD along the vertical axis. The flotor of a MLHD has 6 coils. Each coil lies between a fixed magnet assembly as shown in Fig. 4. Current is passed through each of these coils. Lorentz forces are generated where the current loops of the six actuator coils intersect with the magnetic flux loops. Hence, the magnetic field and thereby the Lorentz forces obtained from the coil currents are dependent on the position of the coil in the air gap. Due to the large air gap in each magnet assembly these fields are not uniform in the given workspace, which leads to a nonlinear force vs. displacement curve [3].

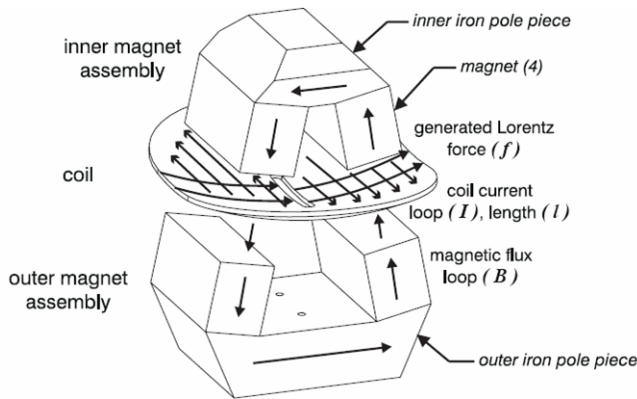


Figure 4: Single magnet assembly within a MLHD.

A physical setup was built to calibrate the MLHD along the vertical axis, as shown in Fig. 5. The setup consisted of a micron resolution linear stage holding a force gauge, aluminium structures and face plates. The flotor was then levitated by commanding a feedforward force in a mode where all the axes besides the vertical axis are locked. The feedforward force was set at a value greater than that required to counter the weight of the flotor. The net weight of the flotor and a pair of plates attached to the handle of the MLHD was measured as 8.58N. The base of the setup was then placed on

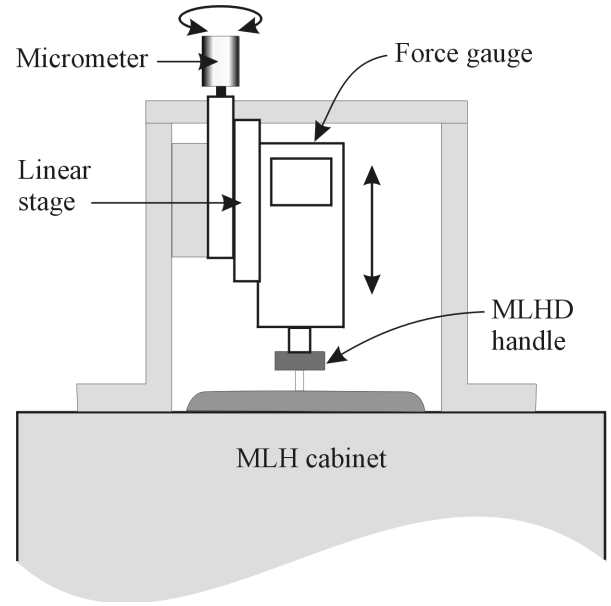


Figure 5: Sketch of calibration setup.

top of the MLHD and the force gauge was lowered such that the tip of the force gauge rested on the plate attached to the handle of the MLHD. The purpose of the plate was to provide a rigid and flat surface for the tip of the force gauge. The force gauge is then lowered by a millimeter at a time using the linear stage. The reading on the force gauge and the values given by the position sensors of the MLHD were noted. These readings were noted for a traversal of 14mm along the vertical axis. Two iterations of feedforward values of 10N and 12N each were made. This gave four force versus displacement curves. Had the magnetic fields of the MLHD been uniform in the given workspace, the force readings would have been a constant value of the difference between the commanded feedforward force and the weight of the flotor. However, the error caused by the nonlinearity was found to be approximately 10.87%.

Each of the four curves were first denormalised by subtracting their means. Next, the nonlinear error curve was parameterized by fitting a second-degree polynomial function to it. This normalised polynomial is as shown in Fig. 6 and is expressed as

$$p(x) = -0.00451x^2 - 0.02583x + 0.19157, \quad \text{where} \quad (20)$$

x is the normalised displacement. In order to be applied to the runtime unnormalised force values, $p(x)$ was denormalised by adding the mean value of each curve to itself. This mean value is unknown during run-time. Hence, it was approximated as the commanded feedforward force. When the denormalised polynomial curve is inverted and multiplied by the calculated vertical force values, a straight line at ~ 1 is obtained. Hence, it is then multiplied by the mean force value or the commanded feedforward force. The final equation for calibration is

$$P_{calibrated} = \frac{P \times FF}{p(x) + FF}, \quad \text{where} \quad (21)$$

FF is the commanded feedforward force.

3.3 Visual Rendering

The spring coil was built in three stages: (1) definition of the spring centerline based on Lowery's model, (2) definition of a helical curve based on the spring centerline, and (3) definition of a helix

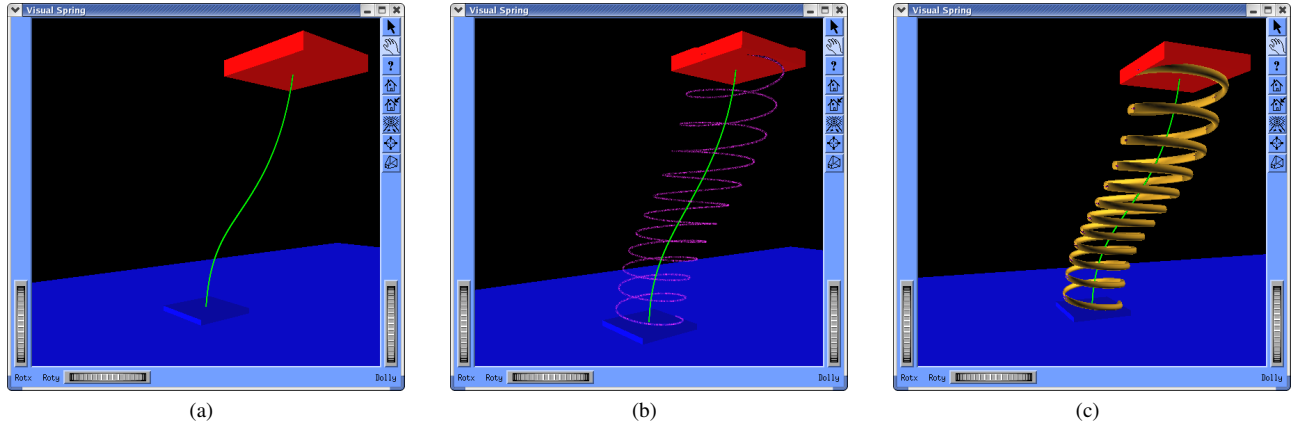


Figure 7: Building a visual spring: (a) Spring centerline (b) Helical curve (c) Helix with a circular cross-section.

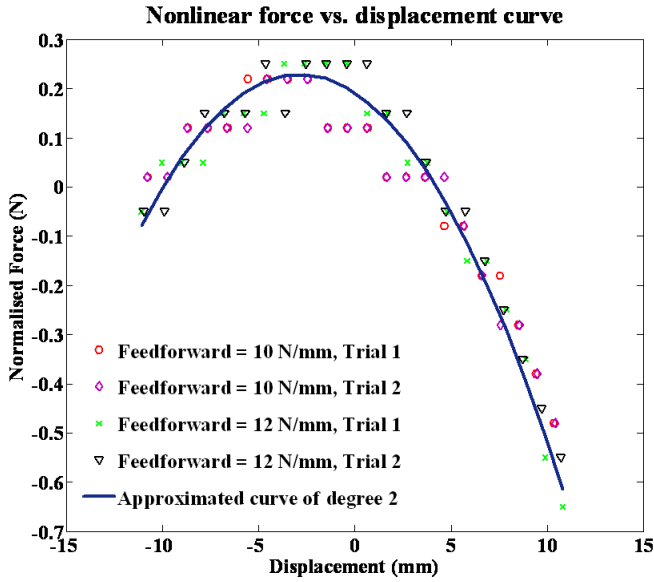


Figure 6: Nonlinear Error Curve.

with a circular cross-section based on the helical curve, as shown in Fig. 7. These definitions are used to update the graphics at a rate of 30 Hz. The graphics of the 3D spring was rendered using Open Inventor [7]. The transformation of the translation data captured by the sensors, and the calculation of the vertical force, horizontal forces and resisting moments are identical to those used for haptic rendering. The 3D coordinates of each point in the spring centerline during compression are given by

$$C_Y = \frac{i * L}{2n\pi}, \quad i : 0 \rightarrow 2n\pi, \quad \text{and} \quad (22)$$

$$C_{X,Z} = \frac{1}{P} \left[M_{U_{z,x}} \left(\tan \left(\frac{qL}{2} \right) \sin(qC_Y) + \cos(qC_Y) - 1 \right) + H_{X,Z} L \left(\frac{-\sin(qC_Y)}{\tan(qL)} + \cos(qC_Y) + \frac{C_Y}{L} - 1 \right) \right]. \quad (23)$$

The coordinates during elongation were derived as

$$C_{X,Z} = \frac{1}{P} \left[M_{U_{z,x}} \left(-\tanh \left(\frac{qL}{2} \right) \sinh(qC_Y) + \cosh(qC_Y) - 1 \right) + H_{X,Z} L \left(\frac{-\sinh(qC_Y)}{\tanh(qL)} + \cosh(qC_Y) + \frac{C_Y}{L} - 1 \right) \right]. \quad (24)$$

These values also undergo a transformation of axes through ψ_{L_z} and then through ψ_{L_x} . A helix of diameter D with each point in its centerline having coordinates $\{C_X, C_Y, C_Z\}$ is then defined. The helix was rendered using a NURBS curve that coiled around the spring centerline. The circular cross-section was rendered by connecting corresponding points of circles defined about each point in the helical curve. The number of points in the spring centerline are large enough to render a seamless helix and small enough to render a real-time simulation on an AMD XP 2000+ computer with a nVIDIA GeForce4 TI 4600 graphics card.

4 PSYCHOPHYSICAL EXPERIMENTS

Implementation of an analytical model of the spring allowed for easy modification of the spring parameters. Such a spring can be defined either in terms of its physical properties (L_0, n, d, D, E , and G) or in terms of its rigidity constants (α, β, γ). These values are manipulated using Graphical User Interfaces as shown in Figs. 8 and 9. The panel in Fig. 8 also allows change in control parameters such as proportional and dampening constants. These parameters determine the translational and rotational limits of the spring and the behavior of the spring at these limits.

It can be seen from eqns. (5), (6), and (7) that α and β vary only with γ if D, G and E were assumed to be constant. Using this property, two psychophysical experiments, Spring Stiffness Magnitude Estimation and JND of Spring Stiffness, were implemented using springs of varying γ . Two modalities were presented in each experiment: vision and haptics (VH), where the subject could see a graphic representation of the haptic spring, and haptics-alone (H), where the window displaying the visual spring was hidden. The visual spring did not change in appearance (e.g., coil thickness or length) with change in γ to prevent the use of visual size and shape cues. However, the visual spring does reflect the motion and deformable characteristics of the haptic spring. The subjects were allowed to modify their view of the visual spring by zooming in or out, rotating the spring about its vertical axis, and changing the angle of inclination of the plane upon which the spring rested. The subjects wore headphones playing white noise during the experiments to minimize auditory influences. A warning in the form of

a beep (audible over the noise) and printed message was given if the subject applied a force against the virtual boundary sufficient to push the flotor out of the device's sensor range.

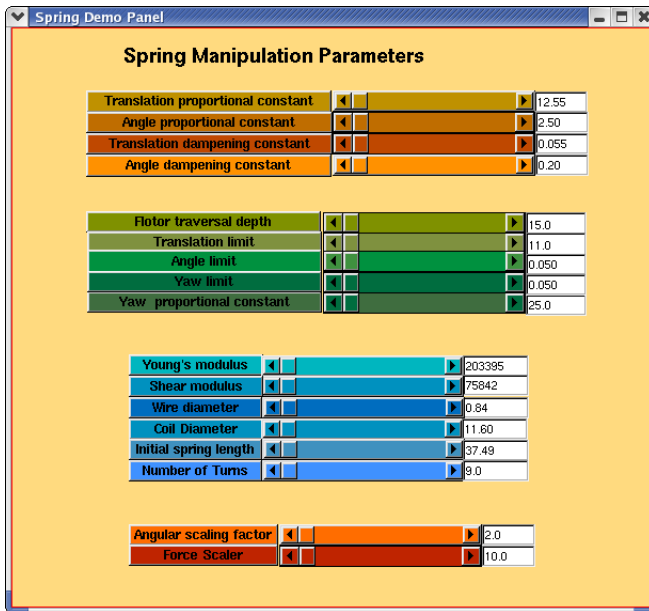


Figure 8: Panel for modifying physical parameters.

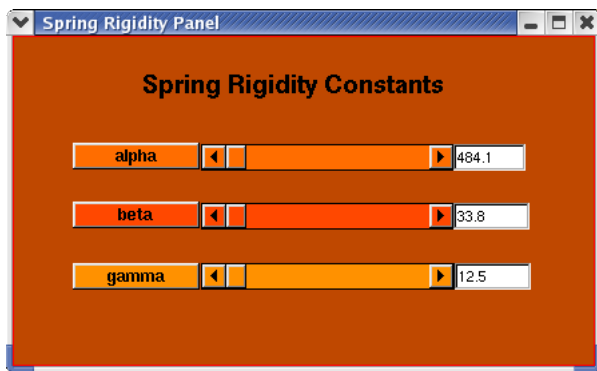


Figure 9: Panel for modifying rigidity constants.

4.1 Spring Stiffness Magnitude Estimation

Sixteen students (6 females and 10 males) from Carnegie Mellon University served as subjects. Two were left-handed and the rest were right-handed by self-report. Eight of the subjects started in the VH modality and the rest started in the H modality, constituting an order variable.

Twelve springs with γ ranging uniformly from 12.0 N to 48.0 N, corresponding to k ranging uniformly from 0.48 N/mm to 1.92 N/mm for $L_0 = 25.0$ mm and natural frequency ranging from 4.57 Hz to 9.16 Hz for a flotor mass of 580 g, were presented to each subject in random order. A subject started in a particular modality and went through three replications of the 12 randomly ordered springs and was then presented with three replications in the other modality. Each set of replications was preceded by a demo of 5 springs in the same modality, sampled from the range of γ s experienced and included the maximum and minimum values of γ . The subject was asked to rate the springs using any number, with the rule

that a higher number meant that the spring felt stiffer. Only positive rational numbers were allowed. The range was self-selected by the subject; analysis of the data included normalization to account for inter-subject variability in the range. With 3 replications of 12 γ values in two modalities, there were 72 trials total, lasting approximately 20 minutes.

4.2 Just Noticeable Difference of Spring Stiffness

Sixteen students (7 females and 9 males) from Carnegie Mellon University served as subjects. Two were left-handed and the rest were right-handed by self-report. Eight of the subjects started in VH modality and the other eight started in H modality, constituting an order variable.

A version of Kaernbach's unforced weighted up-down adaptive threshold estimation was used to rapidly determine the JND [10]. According to this technique, subjects are asked to compare between a base γ_B and a comparison γ_C . A correct decision reduces the difference δ between γ_B and γ_C by stepsize $D1$. An incorrect decision increases δ by a stepsize of $D2$, and an indeterminate answer increases δ by a stepsize of $D3 < D2$. These values were proportional to $D1$ specified by the algorithm with a goal of converging to an accuracy of 75%. The initial value of $D1$ was chosen as 25% of the initial δ , which was chosen as 40% of γ_B ; these values were pre-tested to confirm convergence in a reasonable time. Under the algorithm, as the experiment progresses, γ_C moves towards γ_B and reaches an equilibrium after a certain number of reversals in the direction of δ . The stepsizes are halved at the 2nd and 4th reversals. Equilibrium is assumed after occurrence of the 8th reversal and the JND is calculated as the mean of all δ s between the 4th and the 8th reversal.

The experiment consisted of 3 γ_B s of 17.0 N, 26.0 N and 35.0 N, corresponding to k s of 0.68 N/mm, 1.04 N/mm and 1.4 N/mm for $L_0 = 25.0$ mm and natural frequencies of 5.45 Hz, 6.74 Hz and 7.82 Hz for a flotor mass of 580 g. Four replications of alternating modalities were conducted per subject. The base values followed a non-repeating Latin-square order between replications, and the order within a replication was randomly chosen from the 6 possible permutations. The experiment was preceded by a demo of 4 springs in each modality in mixed order, which together sampled the range of γ and the types of comparisons (one spring obviously stiffer than the other, one spring close but distinguishable from the other, two very similar springs) the subject would experience. The experiment took approximately 1 hour per subject, during which the subject felt about 200 pairs of springs.

5 RESULTS

5.1 Spring Stiffness Magnitude Estimation

For the magnitude estimation task, the normalized magnitude rating were analyzed with an ANOVA on modality (2, VH and H), order (2: VH first; H first), and γ (12). The effect of modality did not approach significance [$F(1, 14) < 0.02, p = 0.88$] nor was the effect involving order significant [$F(1, 14) < 0.823, p = 0.198$]. The sole effect was that of γ [$F(11, 154) = 13.57, p < 0.001$]. This reflected an increase in judged magnitude with rendered γ that was essentially linear (R^2 for linear trend = 0.983), as shown in Fig. 10. The magnitude estimation data follows the power law with an exponent of 0.925.

The positions of the handle and forces applied by the subjects during the experiment were recorded at 1000 Hz. From these data, the variables of mean velocity, acceleration and force along the vertical axis were analyzed with an ANOVA on γ (12), and modality (2, VH and H). The effect of γ was clearly seen in the variables of mean velocity [$F(11,77) = 9.25, p < 0.001$], acceleration [$F(11, 77) = 3.73, p < 0.001$], and force [$F(11,77) = 11.92, p < 0.001$] along the vertical axis as shown in Figs. 11 - 13. Specifically, velocity

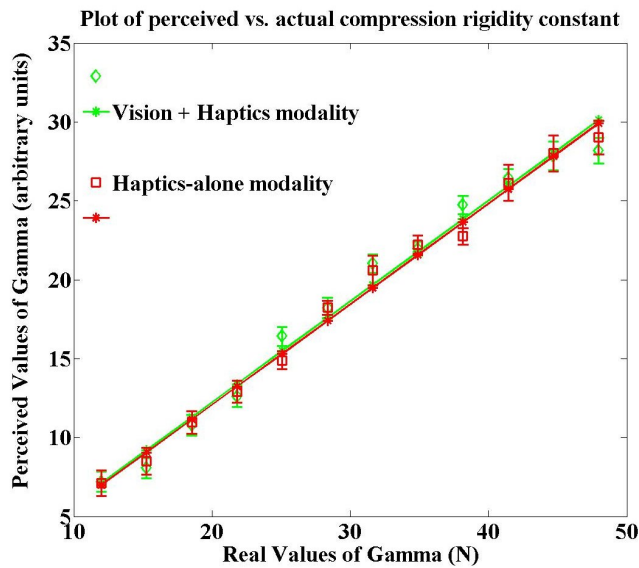


Figure 10: Plot of perceived γ vs. real γ in Vision+Haptics and Haptics-alone modalities.

and acceleration are inversely proportional and force is directly proportional to the rendered γ . All three variables show linear trends with respect to γ (R^2 for linear trend = 0.928, 0.718, and 0.946, respectively). However, these three variables were not affected by modality.

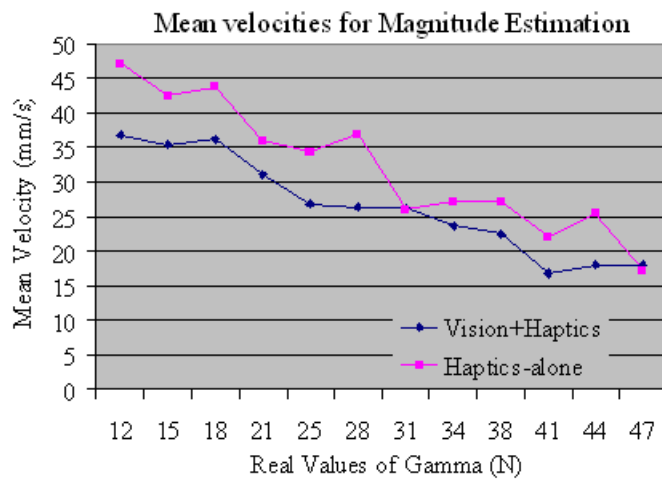


Figure 11: Plot of mean velocity vs. real γ in Vision+Haptics and Haptics-alone modalities.

5.2 Just Noticeable Difference of Spring Stiffness

For the JND task, the threshold values were analyzed with an ANOVA on modality (2, VH and H), γ_B (3), and order (2: VH first; H first). This analysis showed effects of modality [$F(1, 14) = 11.94$, $p = 0.004$] and γ_B [$F(2, 28) = 23.01$, $p < 0.001$] as shown in Fig. 14, but no significant effect involving order.

The hypothesis that the JND is a constant fraction of γ_B for each modality would predict a modality by γ_B interaction, which approached significance [$F(2, 28) = 3.10$, $p = 0.061$]. In a subsidiary analysis testing this hypothesis, it was found that JND expressed

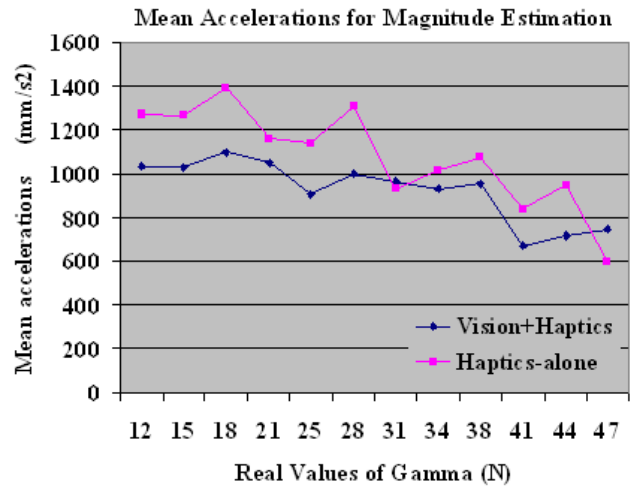


Figure 12: Plot of mean acceleration vs. real γ in Vision+Haptics and Haptics-alone modalities.

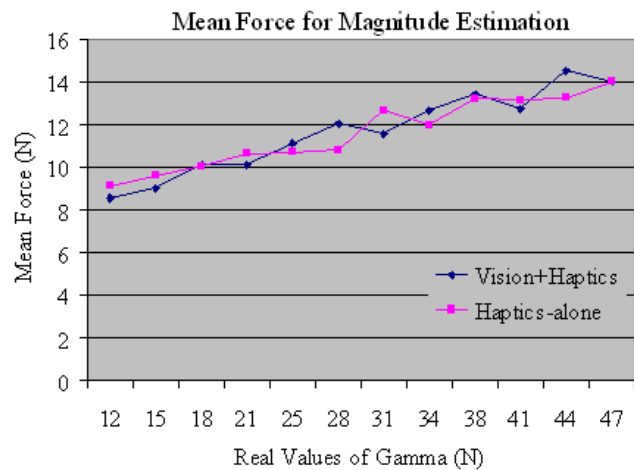


Figure 13: Plot of mean force along vertical axis vs. real γ in Vision+Haptics and Haptics-alone modalities.

as a proportion of γ_B was statistically invariant across γ_B values for both the VH [$F(2,30) = 1.46$, $p = 0.25$] and H conditions [$F(2,30) = 0.80$, $p = 0.46$]. The average JND as a proportion of γ_B , i.e., the “Weber fraction,” was 14.2% for VH versus 17.2% for H, and these differed reliably [$t(15) = 3.30$, $p = 0.005$ (two-tail)].

The variables of mean velocity, acceleration and force along the vertical axis were analyzed with an ANOVA on γ_B (3), and modality (2, VH and H). The findings were that velocity shows only an effect of γ_B [$F(2,12) = 5.13$, $p = 0.025$], acceleration shows no effect of γ_B or modality, and force shows an effect only of γ_B [$F(2,12) = 13.18$, $p = 0.001$].

6 CONCLUSIONS

From the stated results, it was found that perceived stiffness increased linearly with rendered stiffness across the full range studied here. Clearly, participants in the experiment were able to discriminate and evaluate the rendered stiffness well. The importance of kinesthesia is demonstrated by the finding that as the springs get stiffer, the subjects apply more force and move the spring more slowly. Kinesthesia refers to perception of forces from muscle, ten-

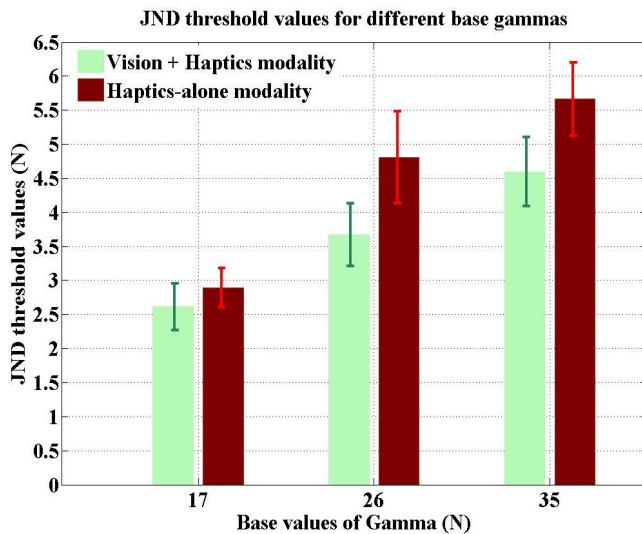


Figure 14: Bar graph of threshold values for different γ_B s in Vision+Haptics and Haptics-alone modalities.

don, and joint receptor input. This means that the level of active control of the spring varied with the rendered γ and implies that it helped in perception of stiffness. Moreover, visual information did not modulate the judged stiffness value, indicating that it relied completely on the haptic rendering.

In contrast, although vision did not affect the sense of stiffness, visual cues did improve people's ability to discriminate between two stiffness values at the difference threshold. The differential stiffness required to discriminate between two springs increased by over 20% if vision was eliminated. The findings that kinesthetic responses in the JND experiment depended only on γ_B and not on modality further imply that visual cues were used to improve the performance in the task of discriminating between springs. A notable finding was the value of Weber fraction for spring stiffness as 14.2% or 1/7 with both visual and haptic sensory information, and 17.2% or 1/5.8 with haptic sensory information alone.

During debriefing of subjects, many of them stated that they explored the spring using vertical oscillatory up and down motions, which agrees with our findings and is predicted in [14]. Some commented that they started making their decisions using a certain strategy, most often compression, and if the comparisons became difficult, they tried an additional strategy such as elongation. The finding that visual cues helped in discrimination suggests that visual observation of the spring's behavior was one such additional strategy. These visual observations would include the frequency of the spring's oscillation after compression or elongation, the buckling length, and the height to which the spring can be elongated. This difference in the use of visual information can be attributed to the precision requirements of the task: In the magnitude estimation experiment, the subject was asked to report the subjective stiffness of each spring in isolation. Differences in the springs were supra-threshold, and no discrimination was required. On the other hand, the task of the JND experiment required fine discriminations, and visual cues clearly added to the discriminative information available.

Almost all subjects commented that the haptic and visual simulations were very realistic. Neither the range of motion of the MLHD nor the inertia of the flotor appears to have affected cases with lower values of γ , given that the exploration data do not show discontinuities. These results demonstrate the effectiveness of a MLHD in rendering a deformable spring.

7 FUTURE WORK

An improved haptic and visual model for post-buckling spring behavior would increase the effectiveness and realism of the simula-

tion. Also, an increase in the limit on the angle of rotation would allow greater exploration of the spring's characteristics. It would be interesting to investigate how people perceive the change in a spring's characteristics, such as stiffness, with respect to changes in physical parameters (L_0, n, d, D, E , and G) and the two other rigidity constants of the spring (α, β). Comparison of the results of the psychophysical experiments with virtual springs to parallel experiments with real springs is an important further step. An additional psychophysical experiment using virtual visual springs alone would contribute toward our understanding of the role of visual cues in perception of spring stiffness.

The simulation of the 3D spring can be used for educational purposes to develop a "feel" for the role of different materials and structural parameters in determining the stiffness and behavior of a helical spring. This work is a concrete example of the ability of a MLHD to render a deformable object based on an analytical model and to quantify human perception of its stiffness.

ACKNOWLEDGEMENTS

This work was partially supported by National Science Foundation grant IIS-0413085. V. Varadharajan was partially supported by a Google Anita Borg scholarship. The authors thank Ben Brown for his assistance with the spring model.

REFERENCES

- [1] J. Barbic and D. L. James. Real-time subspace integration of st.venant-kirchhoff deformable models. In *ACM Transactions on Graphics (ACM SIGGRAPH 2005)*, 2005.
- [2] K. Bathe. *Finite Element Procedures*. Prentice Hall, New Jersey, 1996.
- [3] P. J. Berkelman and R. L. Hollis. Lorentz magnetic levitation for haptic interaction: Device design, performance, and integration with physical simulations. *International Journal of Robotics Research*, Vol. 19, No. 7:644–667, July 2000.
- [4] G. P. Bingham, R. C. Schmidt, and L. D. Rosenblum. Dynamics and the orientation of kinematic forms in visual event recognition. *Journal of Experimental Psychology*, Vol. 21, No. 6:1473–1493, 1995.
- [5] M. de Pascale, G. de Pascale, and D. Prattichizzo. Haptic and graphic rendering of deformable objects based on gpus. In *IEEE 6th Workshop on Multimedia Signal Processing*, 2004.
- [6] A. Frisoli, L. F. Borelli, C. Stasi, M. Bellini, C. Bianchi, E. Ruffaldi, G. D. Pietro, and M. Bergamasco. Simulation of real-time deformable soft tissues for computer assisted surgery. *The International Journal of Medical Robotics & Computer Assisted Surgery*, 1, Issue 1:107–113, 2004.
- [7] S. Graphics, Inc., . E. A. Ave., Sunnyvale, CA, and USA. Open inventor, <http://oss.sgi.com/projects/inventor/>.
- [8] D. L. James and D. K. Pai. Accurate real time deformable objects. In *SIGGRAPH 99 Conference Proceedings*, pages 65–72, 1999.
- [9] D. L. James and D. K. Pai. A unified treatment of elastostatic and rigid contact simulation for real time haptics. *Haptics-e, the Electronic Journal of Haptics Research*, 2, No. 1, 2001.
- [10] C. Kaernbach. Adaptive threshold estimation with unforced-choice tasks. *Perception and Psychophysics*, Vol. 63:1377–1388, 2001.
- [11] R. H. LaMotte. Softness discrimination with a tool. *Journal of Neurophysiology*, Vol. 83:1777–1786, 2000.
- [12] T. M. Lowery. *How to predict buckling and unseating of coil springs*, pages 56–60. McGraw-Hill Book Company, 1961.
- [13] M. Mahvash and V. Hayward. Haptic simulation of a tool in contact with a nonlinear deformable body. In *IS4TM: Int'l Symp. Surgery Simulation and Soft Tissue Modelling*, pages 311–320. Springer Verlag, 2003.
- [14] M. A. Srinivasan and R. H. LaMotte. Tactile discrimination of softness. *Journal of Neurophysiology*, Vol. 73, No. 1:88–101, 1995.
- [15] P. Volino, P. Davy, U. Bonanni, C. Luble, N. Magnenat-Thalmann, M. Mkinen, and H. Meinander. From measured physical parameters to the haptic feeling of fabric. *The Visual Computer: International Journal of Computer Graphics*, Vol. 23, Issue 2:133–142, 2007.
- [16] W. Wu, C. Basdogan, and M. A. Srinivasan. Visual, haptic, and bimodal perception of size and stiffness in virtual environments. *ASME Dynamic Systems and Control, DSC-Vol. 67:19–26*, 1999.